Physicochem. Probl. Miner. Process., 62(2), 2026, 220816

http://www.journalssystem.com/ppmp

Physicochemical Problems of Mineral Processing

ISSN 1643-1049

Amino acid-based surfactant for enhanced scandium (Sc) recovery from red mud: Kinetics and interfacial thermodynamics

Zuhrina Masyithah [1], Widharta Surya Alam [1,2,3], Sabila Gitamara [1]

[1] Department of Chemical Engineering, Faculty of Engineering, Universitas Sumatera Utara, Medan, Indonesia

[2] Department of Chemical Engineering, Faculty of Engineering, Universitas Gadjah Mada, Yogyakarta, Indonesia

[3] Sustainable Mineral Metallurgical Processes Research Group, Faculty of Engineering, Universitas Gadjah Mada, Yogyakarta, Indonesia

Corresponding author: zuhrina.masyithah@usu.ac.id (Zuhrina Masyithah)

Abstract: The accumulation of red mud, a highly alkaline byproduct of alumina production, poses a persistent environmental challenge while containing valuable rare-earth elements such as scandium (Sc). This study introduces an amino acid-based surfactant (AAS) synthesized via direct amidation between coconut oil-based fatty acid (COFA) and L-tryptophan using ZnO as a heterogeneous catalyst, offering a biodegradable and non-toxic alternative to conventional surfactants for enhanced scandium recovery from red mud. Interfacial thermodynamic analysis of AAS confirmed spontaneous and entropy-driven micellization and adsorption (ΔG_{mic} = −18.7 kJ mol^{-1}; ΔG_{ads} = −27.5 kJ mol^{-1}). Application of AAS in scandium recovery from red mud using H_2SO_4 achieved 73.9% Sc extraction and a selectivity ratio (X_{Sc}/X_{Fe}) of 1.33, surpassing cetyltrimethylammonium bromide (CTAB) and blank systems. Kinetic analysis revealed a mechanism transition from surface reaction to diffusion control, supported by an activation energy of 29.5 kJ mol^{-1}. Structural and mineralogical analyses (BET–BJH and XRD) verified that AAS preserved the Fe matrix while promoting selective Sc dissolution. Furthermore, a preliminary technoeconomic analysis (TEA) revealed that the AAS-assisted process is more cost-effective than conventional methods, achieving a unit production cost of 3.72 USD/g Sc_2O_3. Environmental impact assessment (EIA) confirmed that AAS is significantly safer and more biodegradable than CTAB, with an LC_{50} value of 200–484 mg/L, representing a 667–1,613-fold reduction in ecological toxicity.

Keywords: red mud, scandium, leaching kinetics, amino acid surfactant, thermodynamics

1. Introduction

Red mud is the primary solid hazardous waste generated from alumina (Al_2O_3) production via the Bayer process. With a generation rate of 1–2 tons per ton of Al_2O_3, this highly alkaline residue (pH>12) poses significant environmental risks due to the presence of heavy metals and the lack of large-scale management strategies (Klauber et al., 2011; Lan et al., 2025). However, red mud represents a substantial economic opportunity as a secondary resource for critical raw materials, particularly scandium (Sc), yttrium (Y), and other rare earth elements (REEs). Among these, scandium is the most strategic, contributing up to 95% of the total economic value of critical metals in bauxite residue despite its trace concentration (Kanekaputra and Mubarok, 2023; Li et al., 2022). Given that global scandium demand for solid oxide fuel cells (SOFCs) and advanced alloys is rising while natural supply remains scarce (<22 ppm in Earth's crust), recovering Sc from red mud, which typically contains 50–140 ppm, is of high strategic importance (Borra et al., 2016a; Borra et al., 2016b; Rivera et al., 2017; Shoppert et al., 2022).

Various hydrometallurgical methods, including high-pressure acid leaching (HPAL), organic complexation, and alkali fusion, have been employed to extract REEs. While effective, these methods often suffer from high energy consumption, poor selectivity against iron (Fe), and diffusion limitation due to reverse adsorption of REE into red mud pores (Kanekaputra and Mubarok, 2023; Shoppert et al., 2022; Zhou et al., 2018). To address these constraints, surfactants have been introduced as leaching

DOI: 10.37190/ppmp/220816

promoters. Conventional surfactants like sodium dodecyl sulfate (SDS), cetyltrimethylammonium bromide (CTAB), and sodium alcohol ether carboxylate (AEC-9Na) can reduce surface tension and enhance leachate penetration into mineral micropores (Lan et al., 2025; Zhang et al., 2021; Zhou et al., 2023). However, the application of these synthetic surfactants is often limited by their toxicity to aquatic life, poor biodegradability, and sensitivity to multivalent ions in complex leachate solutions (Timmer et al., 2019; Welch et al., 2021).

These limitations have driven the search for green alternatives, specifically amino acid-based surfactants (AAS). AAS molecules, characterized by amine and carboxylate headgroups, offer a unique combination of biodegradability, low toxicity, and the ability to interact with metal species via electrostatic and hydrogen bonding (Kalebic et al., 2023; Niu et al., 2022). Specifically, AAS synthesized from L-tryptophan and fatty acids is promising due to the indole ring structure, which may enhance interfacial stability through л–л interactions (Hafidi et al., 2025).

Despite the potential of AAS, its application in red mud leaching remains largely unexplored. To date, there is no comprehensive study investigating the interfacial thermodynamics of AAS in sulfuric acid systems or its influence on the reaction mechanisms of scandium recovery. Therefore, this study aims to synthesize a novel AAS from L-tryptophan and coconut oil-based fatty acid (COFA), characterize its interfacial properties, and evaluate its performance in enhancing scandium leaching from red mud. By applying the Shrinking Core Model (SCM) to analyze the kinetic data, this work seeks to elucidate the rate-controlling steps and demonstrate the potential of AAS as an eco-friendly promoter for sustainable critical metal recovery.

2. Materials and methods

2.1. Materials

The primary precursors used in this study were L-tryptophan (CheilJedang Corp., Korea) and coconut oil-based fatty acid/COFA (Barco™). COFA served as a source of C_{12}–C_{14} fatty acids, while L-tryptophan provided an amine head group. The amine acylation reaction was conducted using ZnO as a heterogeneous catalyst, with n-hexane and isopropanol as solvents. Product purification was carried out via extraction using an acetone-citric acid system (Holemberg et al., 2025). In the context of hydrometallurgical application, red mud samples from alumina refinery located in Kalimantan, Indonesia, and sulfuric acid (H_2SO_4) was employed as the leaching agent (lixiviant). Scandium quantification was performed using a certified scandium (Sc) CRM standard ICP (*Trace*CERT®, 1000 ppm). A commercial surfactant, cetyltrimethylammonium bromide (CTAB), was used as a benchmark. Unless otherwise stated, all chemicals and analytical-grade solvents were supplied by Sigma-Aldrich Merck™ (Darmstadt, Germany).

2.2. Synthesis of amino acid-based surfactant (AAS)

Amino acid-based surfactant (AAS) was synthesized via direct catalysis of L-tryptophan and coconut oil-based fatty acid (COFA). The reaction was carried out in a 500 mL batch reactor equipped with an agitator and reflux condenser at solvent-reactant (S/R) (g/g). Kinetic experiments were conducted at temperatures of 60, 70, and 80 ^{o}C, with ZnO catalyst loadings of 3, 5, and 7 wt%, and mole ratio amino acid and fatty acid (A/TG) at 2/1, 4/1, and 6/1 (Alam et al., 2022; Holemberg et al., 2025). Reaction samples were withdrawn every 30 min up to 200 min and analyzed to determine fatty acid conversion using chromatographic methods (GCMS Shimadzu QP2010SE), followed by computational processing.

2.3. Characterization of synthesized amino acid-based surfactant (AAS)

The synthesized amino acid-based surfactant (AAS) was characterized to confirm its molecular structure and interfacial charge behavior. Fourier Transform Infrared (FTIR) spectroscopy (Shimadzu IRPrestige-21, 3500–500 cm^{-1}) was employed to identify the functional groups formed during the amidation reaction between L-tryptophan and fatty acids. Structural confirmation was further performed by ^{1}H Nuclear Magnetic Resonance (^{1}H-NMR) spectroscopy (Bruker Avance 400 MHz NMR spectrometer).

2.4. Interfacial thermodynamic analysis

The interfacial properties of AAS were evaluated using surface tension (γ) measurements at concentrations of 0.024–0.1 mol L^{-1} and temperatures of 30, 50, and 70 °C, measured with a du Noüy tensiometer (Cole Parmer Surface Tensiomat 21). The critical micelle concentration (CMC) was determined from the γ–log C plots (Javed et al., 2022). The associated interfacial thermodynamic parameters were calculated based on the Gibbs adsorption framework (Eq. 1 to 7):

$$\Gamma_{max} = -\frac{1}{2.303\,RT}\left(\frac{\partial \gamma}{\partial \log C}\right) \quad (1)$$

$$A_{min} = \frac{1}{N_A \Gamma_{max}} \quad (2)$$

$$\Delta G_{mic} = RT \ln X_{CMC} \quad (3)$$

$$\Delta G_{ads} = \Delta G_{mic} - \frac{\Pi_{CMC}}{\Gamma_{max}} \quad (4)$$

$$\Pi_{CMC} = \gamma_0 - \gamma_{CMC} \quad (5)$$

$$\Delta G_{mic} = \Delta H_{mic} - T\Delta S_{mic} \quad (6)$$

$$\Delta G_{ads} = \Delta H_{ads} - T\Delta S_{ads} \quad (7)$$

Interfacial thermodynamic parameters, including maximum surface excess (Γ_{max}), minimum molecular area (A_{min}), Gibbs free energies of micellization (ΔG_{mic}) and adsorption (ΔG_{ads}), and surface pressure at CMC (Π_{CMC}), were calculated based on the Gibbs adsorption isotherm. The temperature dependence of micellization and adsorption was analyzed using the Gibbs–Helmholtz relationship to obtain enthalpy (ΔH) and entropy (ΔS) changes. All parameters were determined by least-squares regression.

2.5. Hydrometallurgical recovery of scandium (Sc) from red mud

The leaching experiments were performed to evaluate the effectiveness of AAS as a leaching promoter for the recovery of scandium (Sc) from red mud. The process was conducted in a mechanically stirred batch reactor using H_2SO_4 at 40, 60, and 80 °C, with a solid-to-liquid ratio of 10:1, stirring speed of 600 rpm, and leaching time of 120 minutes. Red mud particle size was maintained below 75 µm, and the AAS concentration was kept below its CMC.

The performance of AAS was assessed in comparison with a blank system (without surfactant) and a system containing cetyltrimethylammonium bromide (CTAB) as a commercial reference surfactant. Liquid samples were periodically withdrawn (0–120 min), filtered, and analyzed to determine the dissolved scandium concentrations. The scandium recovery (X_{Sc}) was calculated using Eq. 8.

$$X_{Sc,\,\text{leached}}(\%) = \frac{m_{Sc,\,\text{leached}}}{m_{Sc,\,\text{leached}} + m_{Sc,\,\text{residue}}} \times 100 \quad (8)$$

Scandium concentration in the leachate was measured using Inductively Coupled Plasma- Mass Spectrometry (ICP-MS 2040LF). Iron recovery (X_{Fe}) was calculated using the same mass balance approach based on measuring Fe concentrations. Selectivity toward Sc was evaluated using the recovery ratio of scandium to iron (selectivity ratio = X_{Sc}/X_{Fe}). All experiments were conducted in triplicate, and the reported values represent the average final values.

Phase composition and mineralogical changes of red mud before and after leaching were analyzed using X-Ray Diffraction (XRD, PANalytical). Textural properties, including specific surface area, pore volume, and pore size distribution, were determined by N_2 adsorption-desorption using Brunauer-Emmett-Teller (BET) and Barrett-Joyner-Halenda (BJH) methods (Micromeritics ASAP 2020).

2.6. Mathematical modeling

2.5.1. Reaction kinetics of AAS synthesis

AAS synthesis kinetics were described using a pseudo-Langmuir model analogy to account for reactant saturation on the heterogeneous ZnO catalyst (Liu et al., 2019; Islam et al., 2022). The kinetic modeling and its verification method was expressed Eq. 9 to 13.

$$\frac{dX_A}{dt} = \frac{kC_{A0}(X_{A_{eq}} - X_A)}{1 + KC_{A0}(X_{A_{eq}} - X_A)} \quad (9)$$

$$X_A = \frac{C_{A0} - C_{A(t)}}{C_{A0}} \quad (10)$$

$$X_{Aeq} = \frac{C_{A0} - C_{Aeq}}{C_{A0}} \quad (11)$$

$$R^2 = 1 - \frac{\sum_{i=1}^{n}\left(X_{A,i}^{exp} - X_{A,i}^{model}\right)^2}{\sum_{i=1}^{n}\left(X_{A,i}^{exp} - \overline{X_A}^{exp}\right)^2} \quad (12)$$

$$SSE = \sum_{i=1}^{n}\left(X_{A,i}^{exp} - X_{A,i}^{model}\right)^2 \quad (13)$$

where X_A = FFA conversion (%); k = kinetic rate constant (min^{-1}); K = adsorption constant, C_{A0} = initial reactant concentration (mol L^{-1}), $C_{A(t)}$ = concentration overtime (mol L^{-1}), C_{Aeq} = equilibrium concentration (mol L^{-1}), X_{Aeq}= equilibrium conversion; $X_{A,i}^{exp}$ = FFA conversion based on experiment at time -i; $X_{A,i}^{model}$=FFA conversion based on model at time -i; $\overline{X_A}^{exp}$= mean FFA conversion; and n = number of data point. Model parameters were obtained by fitting experimental conversion-time data, and the goodness of fit was evaluated using the coefficient of determination (R^2) and the sum of squared errors (SSE).

2.5.2. Leaching kinetics of scandium recovery from red mud

Scandium leaching kinetics were analyzed using the Shrinking Core Model (SCM). Due to high agitation, elevated temperature, fine particle size, external mass transfer resistance was neglected (Jodlowski et al., 2017). The kinetics were evaluated using surface chemical reaction control and diffusion through the product (ash) layer (Eq. 14 to 15).

$$1 - (1 - X_{Sc})^{1/3} = k_r . t \quad (14)$$

$$1 - 3(1 - X_{Sc})^{2/3} + 2(1 - X_{Sc}) = k_d . t \quad (15)$$

where X_{Sc} is the scandium recovery (%), k_r and k_d are the rate constants for reaction-controlled and diffusion-controlled mechanisms (min^{-1}), respectively, and t is the leaching time (min). The dominant rate-controlling mechanism was identified by comparing the R^2.

3. Results and discussion

3.1. Reaction kinetics in AAS surfactant synthesis

The reaction kinetics of amino acid-based surfactant (AAS) synthesis were investigated to evaluate the effects of operating parameters on reaction rate and equilibrium conversion (X_{Aeq}). All experimental data were fitted using a pseudo-Langmuir model (Eq. 9) to account for reactant saturation on the heterogeneous ZnO catalyst surface. As shown in Fig. 1 and Table 1, increasing the A/TG molar ratio from 2/1 to 6/1 reduced the rate constant (k) from 0.0032 to 0.0023 min^{-1}, while the adsorption constant (K) increased from 6.856×10^{-2} to 2.581×10^{-1}. These phenomena indicate that excessive amino acid strongly occupies active sites, limiting fatty acid access and suppressing overall conversion.

Temperature exerted a pronounced positive effect, with increasing temperature from 60 to 80 °C

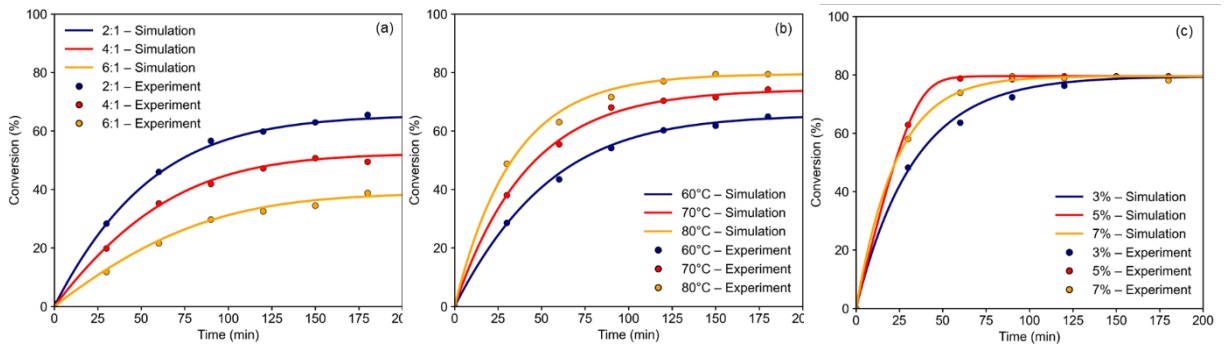

Fig. 1. Reaction kinetics of AAS synthesis: (a) A/TG effect (b) temperature effect (c) catalyst loading effect

Table 1. Parameter fitting of reaction kinetics in AAS synthesis

Variables	Level	Kinetic Parameters		X_{Aeq} (%)	Fitting Quality	
		k (min^{-1})	K		SSE	R^2
Mole Ratio (A/TG)	2/1	0.0032	6.856×10^{-2}	65.51	4.41×10^{-5}	0.9999
	4/1	0.0029	1.595×10^{-1}	52.39	5.70×10^{-5}	0.9997
	6/1	0.0023	2.581×10^{-1}	38.80	2.28×10^{-5}	0.9998
Temperature (^{o}C)	60	0.0032	6.856×10^{-2}	65.51	4.41×10^{-5}	0.9999
	70	0.0034	9.077×10^{-3}	74.42	8.55×10^{-5}	0.9998
	80	0.0041	1.000×10^{-6}	79.50	4.18×10^{-4}	0.9992
Catalyst Loading (%wt)	3	0.0041	1.000×10^{-6}	79.50	4.18×10^{-4}	0.9992
	5	0.0225	$7{,}414 \times 10^{-1}$	79.51	4.14×10^{-6}	1.0000
	7	0.0064	2.109×10^{-2}	79.49	1.81×10^{-4}	0.9996

enhancing k from 0.0032 to 0.0041 min^{-1} and raising conversion to 79.50%. Concurrently, K sharply decreased to 1.000×10^{-6} at 80 ^{o}C, suggesting dominant product desorption and mitigation of surface inhibition. Optimal performance was achieved at a catalyst loading of 5 wt%, yielding the highest k (0.0225 min^{-1}) and excellent fitting accuracy (R^2 = 1.000; SSE=4.14×10^{-6}). The decline in reaction rate at excess catalyst loading confirms that excessive active sites become ineffective due to particle agglomeration (Liu et al., 2019; Islam et al., 2022). Overall, the strong agreement with the pseudo-Langmuir model indicates that AAS amination kinetics are governed by coupled adsorption-reaction processes at the ZnO catalyst interface.

3.2. AAS surfactant characterization

Structural characterization of the AAS by FTIR spectroscopy (Fig. 2a) and ^{1}H-NMR analysis (Fig. 2b) confirm the successful amidation between fatty acid ester groups of COFA and the amine group of L-tryptophan. The AAS spectrum exhibits new characteristic absorption bands at 1640 and 1550 cm^{-1}, corresponding to C=O stretching (amide I) and N-H bending (amide II), respectively, replacing the dominant ester carbonyl peak at 1744 cm^{-1} observed in the COFA precursor.

Further structural validation is provided by ^{1}H-NMR analysis. The AAS spectrum shows integrated aromatic proton signals of the tryptophan indole ring at chemical shifts (δ) of 6.9–7.6 ppm, together with intense upfield multiplets at δ 0.88 and 1.25 ppm. These upfield signals correspond to terminal methyl (–CH_3) and long-chain methylene (–CH_2–) protons originating from the fatty acid hydrophobic tails of COFA, which are absent in the spectrum of pure L-tryptophan (Yamamoto et al., 2009).

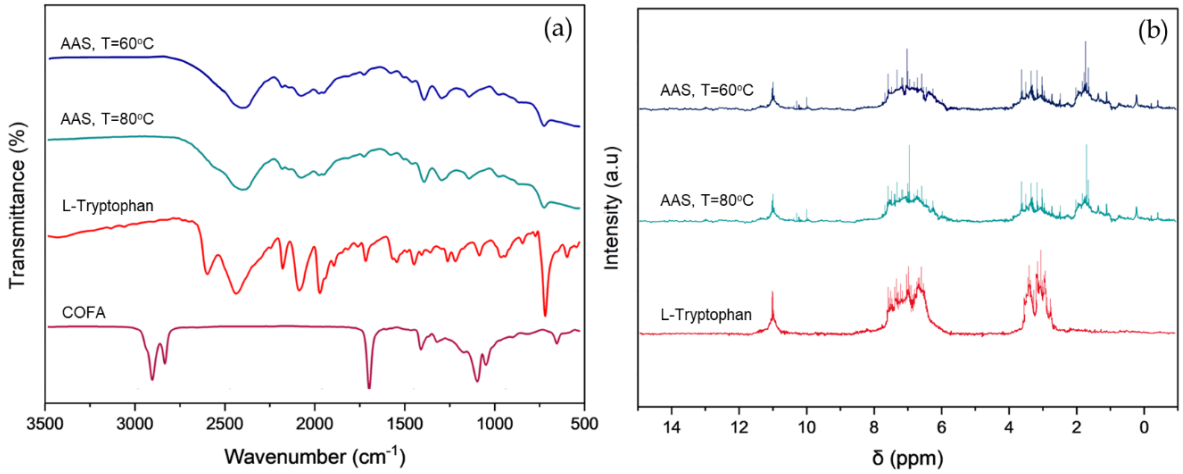

Fig. 2. AAS surfactant characterization: (a) FTIR spectrum (b) ^{1}H-NMR spectrum

The coexistence of aromatic head groups and aliphatic tails verifies the formation of the structure. Sharper signal intensities in samples synthesized at 60–80 ^{o}C indicate higher product conversion, in agreement with the kinetic results.

3.3. AAS surfactant interfacial thermodynamics

The surface tension profile of AAS (Fig. 3a) decreases sharply with concentration and reaches a plateau at the critical micelle concentration (CMC). As summarized in Table 2, increasing temperature from 30 to 70 °C shifts the CMC from 0.05 to 0.08 mol L^{-1}, confirming thermally induced destabilization of micelle formation due to enhanced thermal disruption of water structure surrounding hydrophobic groups.

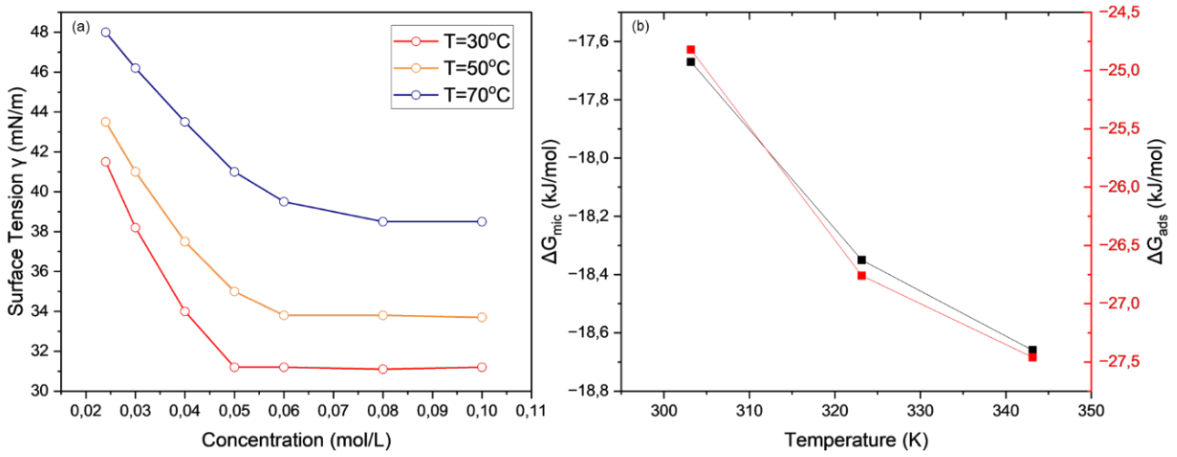

Fig. 3. Interfacial thermodynamics analysis: (a) CMC determination (b) Gibbs free energy of AAS micellization and adsorption across different temperature

Table 2. AAS interfacial thermodynamic parameter analysis

Temperature (°C)	CMC (mol L^{-1})	Γ_{max} (μmol m^{-2})	A_{min} (nm^2)	ΔG_{mic} (kJ mol^{-1})	ΔG_{ads} (kJ mol^{-1})	Π_{CMC} (mN m^{-1})
30	0.05	5.5968	0.2967	−17.6733	−24.8166	39.98
50	0.06	4.0561	0.4094	−18.3494	−26.7590	34.11
70	0.08	2.9463	0.5636	−18.6643	−27.4618	25.92
Process	Enthalpy ΔH (kJ mol^{-1})			Entropy ΔS (J $mol \cdot K^{-1}$)		
Micellization	−10.2225			24.7763		
Adsorption	−4.9758			66.1304		

Thermodynamic analysis (Fig. 3b) shows that the Gibbs free energies of micellization (ΔG_{mic}) and adsorption (ΔG_{ads}) are negative across the entire temperature range, confirming the spontaneous nature of both processes. However, adsorption is thermodynamically favored, with ΔG_{ads} (−24.8 to −27.5 kJ mol^{-1}) being consistently more negative than ΔG_{mic} (−17.7 to −18.7 kJ mol^{-1}) (Kaur et al., 2022). This preference, driven by positive entropy changes (ΔS>0), with the high ΔS_{ads} value 66.13 J mol^{-1} K^{-1} highlights the dominance of hydrophobic effects and underpins the effectiveness of AAS as an interfacial leaching promoter.

3.4. Performance in red mud leaching: scandium recovery and selectivity

The comparative efficiency of scandium extraction is statistically illustrated by box plots in Fig. 4, which evaluate the performance of AAS relative to a commercial cationic surfactant (CTAB) and a blank system. As shown in Fig. 4a and summarized in Table 3, the addition of AAS significantly enhances scandium recovery (X_{Sc}), reaching an average value of 73.93%, compared with 67.76% for CTAB, and 53.51% for the blank system. The relative increase of approximately over the blank is consistent with the well-documented role of surfactants in overcoming kinetic limitations during REE leaching. Previous studies have shown that anionic surfactants such as SDS can reduce solution surface tension by up to 47% (from 72.8 to 38.6 mN m^{-1}), leading to substantial improvements in permeability (up to 4.89×10^{-5} cm s^{-1}) and more effective penetration of lixiviant into mineral micropores (Zhang et al., 2021). A similar enhancement is therefore considered a primary contributor to the higher scandium recovery observed in the presence of AAS.

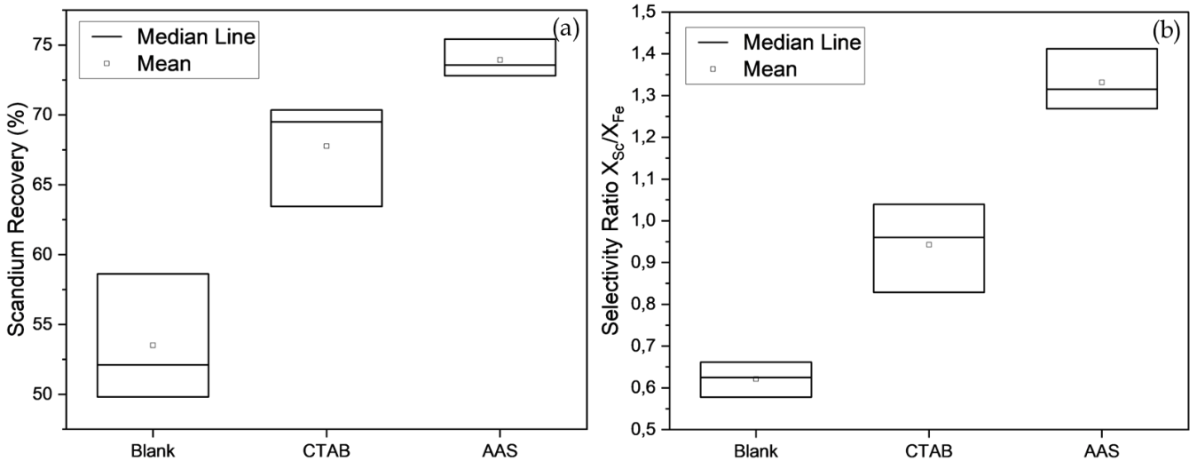

Fig. 4. Performance in red mud leaching; (a) scandium recovery (%); (b) selectivity ratio X_{Sc}/X_{Fe}

Table 3. Summary of performance assessment in red mud leaching

Treatment	Scandium Recovery X_{Sc} (%)	Selectivity Ratio (X_{Sc}/X_{Fe})
Blank	53.51 ± 4.57^{a}	0.62 ± 0.04^{a}
CTAB	67.76 ± 3.76^{b}	0.94 ± 0.11^{b}
AAS	73.93 ± 1.35^{b}	1.33 ± 0.07^{c}

Compared to the blank system, CTAB also improves scandium recovery, which agrees with literature reports implying that low concentrations of CTAB can increase REE recovery from approximately 80% to 90% through enhanced mass transfer and electrostatic interactions at the solid-liquid interface (Zhou et al., 2023, 2024). Beyond extraction efficiency, Fig. 4b highlights the selectivity of scandium leaching over iron. The blank system shows poor selectivity, with X_{Sc}/X_{Fe} ratio of 0.62, indicating significant competitive dissolution of Fe. While CTAB improves this ratio to 0.94, the value remains below unity, reflecting the predominantly non-selective, electrostatic nature of cationic surfactants. Similar limitations have been reported for conventional surfactants, including anionic AEC-9Na, which increases leaching rates of REE by only about 5.2% and exhibits sensitivity towards multivalent ions such as Fe^{3+} and Al^{3+}, often resulting in reduced stability and selectivity (Lan et al., 2025).

In contrast, AAS achieves a markedly higher selectivity ratio of 1.33, corresponding to an increase of more than twofold relative to the blank and CTAB. The indole moiety of L-tryptophan ((2-amino-3-(1H-indole-3-yl)propanoic acid) is reported to enhance interfacial stability through л-л interactions, leading to stronger and more selective adsorption on particle surfaces (Hafidi et al., 2025). This behavior can be rationalized by the presence of the amino-acid structure, which are known to facilitate л- л bonding interactions with REE surfaces (Wu et al., 2013; Kalebic et al., 2023).

The remarkable selectivity (X_{Sc}/X_{Fe}) of AAS arises from a dual-mechanism: wettability enhancement combined with selective iron corrosion inhibition. The surfactant nature of AAS improves acid access to micropores and boosting scandium recovery, while the indole moiety specifically suppresses Fe dissolution. Unlike conventional chelating agents described by hard-soft acid-base theory (HSAB), the indole in AAS as a surface-blocking agent specific to iron minerals. The electron-rich indole ring facilitates strong adsorption onto the more acidic metal center (acidity of $Fe^{3+} > Sc^{3+}$; pK_a $Fe^{3+} < pK_a$ Sc^{3+}), linked to iron oxides (Fe_2O_3) in red mud surface via л-*d* orbital interactions or electrostatic attraction. This forms a hydrophobic protective film that hinders the attack of protons (H^+) on Fe, effectively acting as a corrosion inhibitor (Xiong et al., 2024; Lavanya et al., 2024). Thus, AAS allows effective solubilization of scandium while kinetically passivating Fe, achieving superior separation compared to typical cationic surfactants like CTAB.

Statistical evaluation in Table 3 indicates that both AAS and CTAB yield significantly higher scandium recovery than the blank (shared superscript ^{b} and ^{a}). However, AAS uniquely exhibits a

distinct superscript ([c]) for the selectivity ratio, confirming its statistically superior ability to suppress iron dissolution. This distinctive selectivity demonstrates that AAS operates not only as a surface-active additive but also as a selective agent for scandium with the iron-rich red mud system.

The enhanced scandium selectivity (X_{Sc}/X_{Fe}) observed in the AAS system is primarily governed by a selective suppression of iron dissolution rather than preferential extraction of scandium. This behavior can be understood by integrating interfacial thermodynamics, molecular structure, and mineralogical evidence. As discussed in Section 3.3, the highly negative Gibbs free energy of adsorption ($\Delta G_{ads} < \Delta G_{mic}$) indicates a strong thermodynamic driving force for AAS to accumulate at the solid–liquid interface, promoting the formation of a stable adsorbed layer on mineral surfaces. In addition, the zwitterionic nature of synthesized AAS, confirmed by zeta potential analysis (Fig. 5a), enables dynamic charge adaptation under acidic conditions, allowing the surfactant to maintain effective interaction with both mineral surfaces and dissolved species. The influence of acid concentration on AAS performance can be rationalized through its pH-dependent charge behavior.

Under acidic conditions, the zwiterrionic nature of AAS ensures that this interfacial layer remains stable, enabling sustained interaction with mineral phases. Importantly, the indole functional group exhibits strong affinity toward Fe-rich surfaces, facilitating preferential adsorption onto iron oxides. Unlike conventional cationic surfactants such as CTAB, which possess a fixed positive charge and interact primarily through non-selective electrostatic attraction, AAS exhibits pH-responsive charge adaptability, with an isoelectric point around pH ≈ 5.3. This leads to the formation of a protective surface layer that inhibits proton attack and suppresses Fe dissolution.

In parallel, scandium predominantly exists as soluble Sc^{3+} in simulated Pourbaix diagram, favoring dissolution (Fig. 5b). These combined effects indicate that acid concentration governs both metal speciation and the interfacial behavior of AAS. At sufficiently high acidity, however, changes in intermolecular interactions may influence surfactant organization, suggesting that acid concentration plays a broader role in regulating solution chemistry and surfactant functionality. This explains why the system remains effective under strongly acidic conditions typically used in scandium leaching.

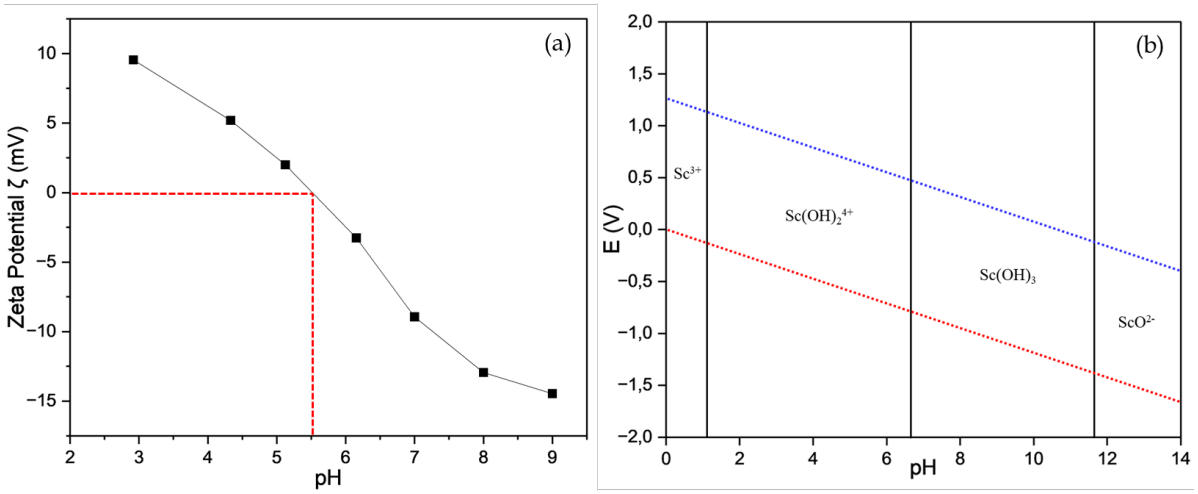

Fig. 5. pH-dependent behavior of AAS and scandium speciation in acidic leaching systems: (a) zeta potential of AAS and (b) Pourbaix diagram of Sc-H-O system

This mechanism is further supported by mineralogical evidence obtained from XRD analysis, which will be discussed in detail in Section 3.6. where the iron mineral phases are largely preserved in the presence of AAS, whereas severe structural degradation is observed in the blank system. In contrast, scandium, which is weaklier bound within the mineral matrix, remains accessible to acid leaching and is readily solubilized. As a result, AAS enables effective scandium extraction while kinetically passivating iron, leading to a significant increase in the selectivity ratio (X_{Sc}/X_{Fe}). Compared to CTAB, which primarily enhances mass transfer through electrostatic interactions, AAS provides an additional layer of molecular-level selectivity through targeted surface interactions and interfacial stabilization, explaining its superior performance.

Such differences highlight the fundamental limitations of conventional surfactants, including anionic, nonionic, and cationic types. Anionic surfactants (e.g., SDS, AEC-9Na) improve wettability but exhibit non-specific interactions, resulting in poor selectivity. Nonionic surfactants are chemically stable yet interact weakly with mineral surfaces. Cationic surfactants such as CTAB rely mainly on electrostatic attraction, which remains blunt selectivity. In contrast, AAS exhibits hybrid interfacial behavior by combining electrostatic interaction, acid-base stability, hydrogen bonding, and specific functional group affinity (e.g., indole), enabling selective adsorption and enhanced Sc/Fe separation.

3.5. The effect of AAS surfactant presence in leaching kinetics and the mechanism

Time-dependent scandium recovery (X_{Sc}) profiles demonstrate that surfactant addition significantly accelerates the initial leaching rate. As shown in Fig. 6a, AAS produces the steepest kinetic slope compared with CTAB and the blank system, suggesting effective reduction of interfacial mass-transfer resistance. In the presence of AAS (Fig. 6b), increasing temperature from 40 to 80°C markedly shortens the time required to reach steady-state scandium recovery, achieving near-equilibrium conditions within 60 min at elevated temperatures. To identify the rate-controlling step, the experimental data were fitted using the Shrinking Core Model (SCM) assuming chemical reaction control (Fig. 7a) and ash-layer diffusion control (Fig. 7b).

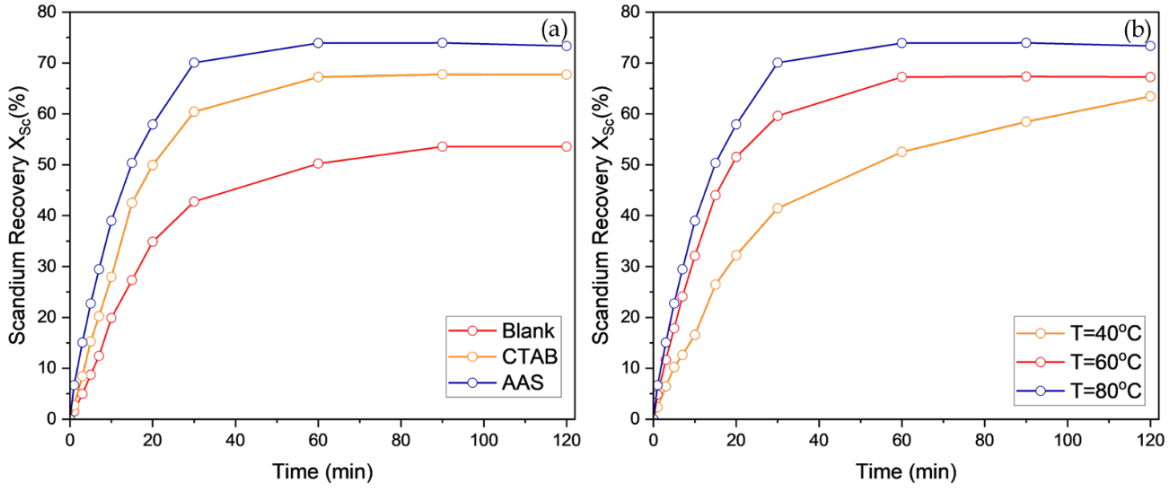

Fig. 6. Scandium leaching profiles as a function of time: (a) effect of surfactant types at 80°C and (b) effect of temperature in the presence of AAS

Fig. 6 clearly demonstrates that the presence of surfactants significantly accelerates the leaching kinetics of scandium compared to the surfactant-free system (blank), as reflected by the steeper increase in Sc recovery at the early stage of leaching. Both AAS and CTAB promote a faster approach to equilibrium recovery, implying a reduction in interfacial and diffusion-related mass transfer limitations during the solid-liquid reaction. These phenomena can be attributed to previous studies reporting that surfactants enhance wettability and improve contact between the leaching solution and mineral surfaces, thereby facilitating metal ion transport into the bulk solution (Ai et al., 2019; Zhang et al., 2021; Zhou et al., 2023).

After prolonged leaching, the recovery curves tend to plateau for all systems, suggesting a transition from kinetically controlled leaching to equilibrium-limited behavior or depletion of readily leachable scandium species. Although recovery profiles approached a plateau at 120 minutes, the kinetic evaluation was focused on the first 30 minutes to capture the dominant interaction dynamics, where the rate of change was highest and differences between samples were most distinguishable prior to equilibrium saturation (Fig. 7 and Fig. 8).

The kinetic parameters summarized in Table 4 reveal a clear difference in the rate-controlling mechanism induced by surfactant presence. In the blank and CTAB systems, leaching kinetics are governed by surface chemical reactions (R^2>0.995), as evidenced by the excellent agreement with the

reaction model (R^2>0.995). This indicates that, under these conditions, the overall leaching rate is limited by the interfacial reaction between H_2SO_4 and scandium-mineral phases.

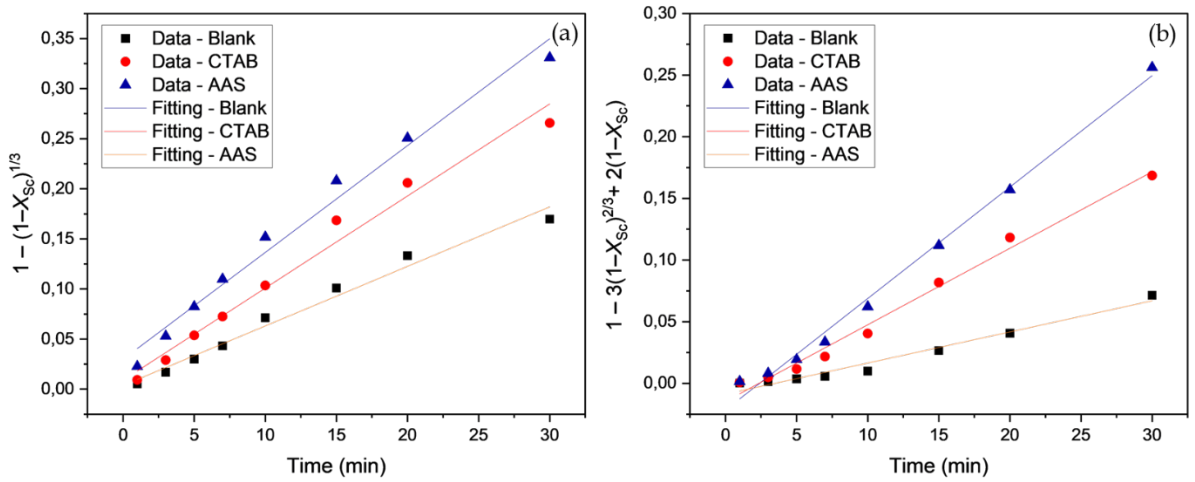

Fig. 7. Shrinking core model (SCM) plots for surfactant variations: (a) chemical reaction control model and (b) ash layer diffusion control model

Table 4. Kinetic parameters for the variation of surfactant presence at 80 °C

Treatment	Reaction Model		Diffusion Model		Mechanism
	k_r	R^2	k_d	R^2	Controlled
Blank	0.0059	0.997	0.0028	0.9898	Reaction
CTAB	0.0064	0.9908	0.0092	0.9954	Diffusion
AAS	0.0107	0.9898	0.0090	0.9977	Diffusion

In contrast, the AAS-assisted system exhibits diffusion-controlled behavior, as evidenced by a superior fitting of the diffusion model (R^2=0.9977). This is consistent with the presence of AAS in significantly enhancing surface reaction kinetics through improved interfacial wetting and accessibility, thereby diminishing chemical reaction resistance. Although both AAS and CTAB were applied at sub-CMC concentrations, their effects on leaching kinetics differed markedly, suggesting that surfactant chemistry rather than concentration alone governs the mechanism. Previous linked studies have reported that surfactant addition enhances leaching performance by improving permeability within porous mineral matrices, thereby accelerating mass transfer processes (Zhou et al., 2023; He et al., 2023).

The temperature-dependent SCM analysis for the AAS system (Fig. 8, Table 5) further supports this interpretation. At 40 °C, leaching remains reaction-controlled (R^2=0.9908), whereas at 60 and 80 °C the mechanism fully shifts to ash-layer diffusion control (R^2>0.988). This transition can be attributed to the strong temperature dependence of surface reaction kinetics, which accelerates rapidly with increasing temperature, thereby diminishing chemical reaction resistance. Once the surface reaction approaches a pseudo-equilibrium state, internal diffusion through the product (ash) layer becomes the dominant rate-limiting step (Oke et al., 2024).

Table 5. Kinetic parameters for the variation of temperature using AAS surfactant

Temperature	Reaction Model		Diffusion Model		Mechanism
(°C)	k_r	R^2	k_d	R^2	Controlled
40	0.0055	0.9908	0.0025	0.9708	Reaction
60	0.0087	0.9662	0.0062	0.9884	Diffusion
80	0.0107	0.9898	0.0090	0.9977	Diffusion

These results confirm the dual role of AAS: (i) accelerating surface chemical reactions through improved interfacial wetting and accessibility, and (ii) facilitating acid penetration into the porous red

mud matrix. Under high-temperature conditions, however, internal diffusion resistance ultimately governs the overall leaching rate.

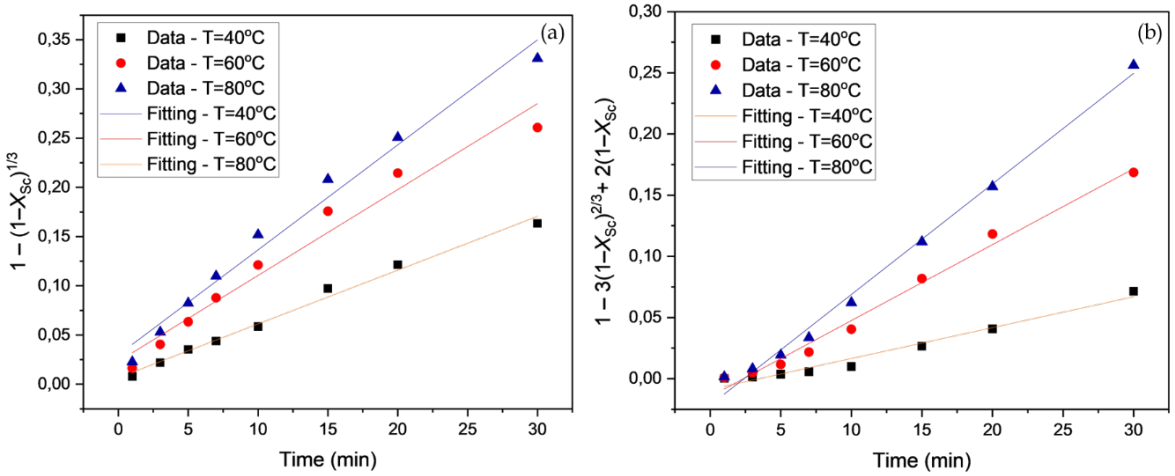

Fig. 8. Shrinking core model (SCM) plots for temperature variations with AAS: (a) chemical reaction control model and (b) ash layer diffusion control model

To provide deeper physical validation of the diffusion-controlled mechanism observed in the AAS system, the activation energy (E_A, kJ mol^{-1}) was determined. The temperature dependence of the diffusion rate constant (k_d) was described using a modified Arrhenius expression for effective diffusion (D_e, m^2 s^{-1}) in Eq. 16 to 17.

$$D_e = D_0 \exp\left(-\frac{E_A}{RT}\right) \tag{16}$$

$$k_d = \frac{6 D_e C_A}{\rho_s R_0} \tag{17}$$

where the effective diffusion coefficient (D_e, m^2 s^{-1}) was derived from k_d through its relationship with particle density (ρ_s, mol m^{-3}), particle radius (R_0, m), and reactant concentration (C_A, mol m^{-3}).

The linearity of the ln D_e versus $1/T$ plot (Fig. 9) yielded an activation energy (E_A) of 29.5 kJ mol^{-1} and a pre-exponential factor (D_0) of 1.1×10^{-9} m^2 s^{-1}.

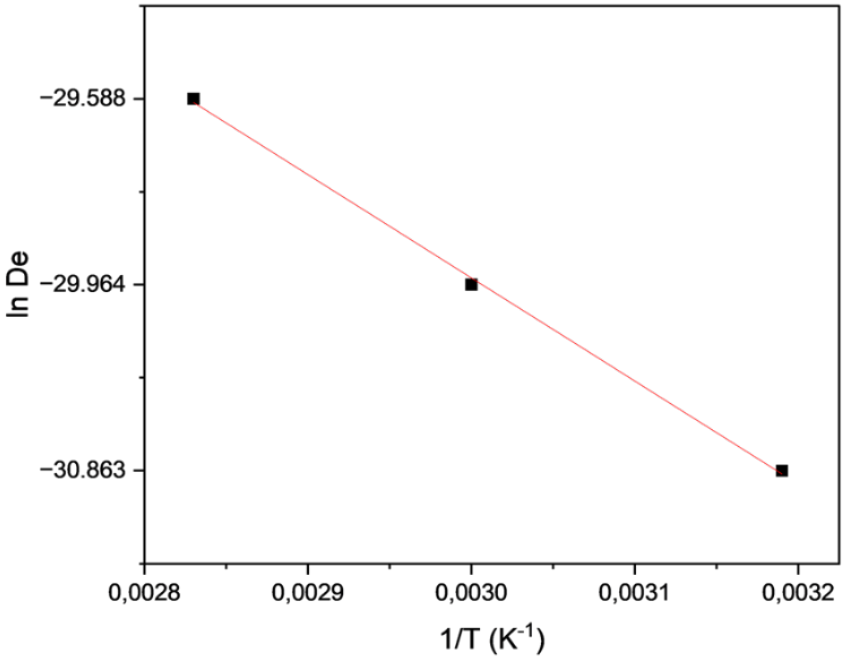

Fig. 9. Linear regression of the Arrhenius plot for determining the activation energy of scandium leaching in the presence of AAS surfactant

Theoretically, chemically controlled processes typically exhibit activation energies (E_A) exceeding 40 kJ mol^{-1}, whereas diffusion-controlled processes are characterized by lower values (Ray et al., 2025). Accordingly, the relatively low E_a obtained provides conclusive evidence that AAS substantially accelerates surface chemical reactions, shifting the rate-determining step entirely toward lixiviant diffusion through the solid product (ash) layer within the red mud matrix.

3.6. Structural and mineralogical transformation analysis

Surface area and pore structure evolution were evaluated using N_2 adsorption-desorption analysis (Fig. 10), with textural parameters summarized in Table 6. All samples exhibited type IV isotherms with H3/H4 hysteresis loops (IUPAC), confirming a mesoporous structure (2-50 nm). Raw red mud showed the lowest N_2 uptake, whereas all leached samples displayed markedly higher adsorption, verifying pore opening and impurity dissolution induced by leaching process.

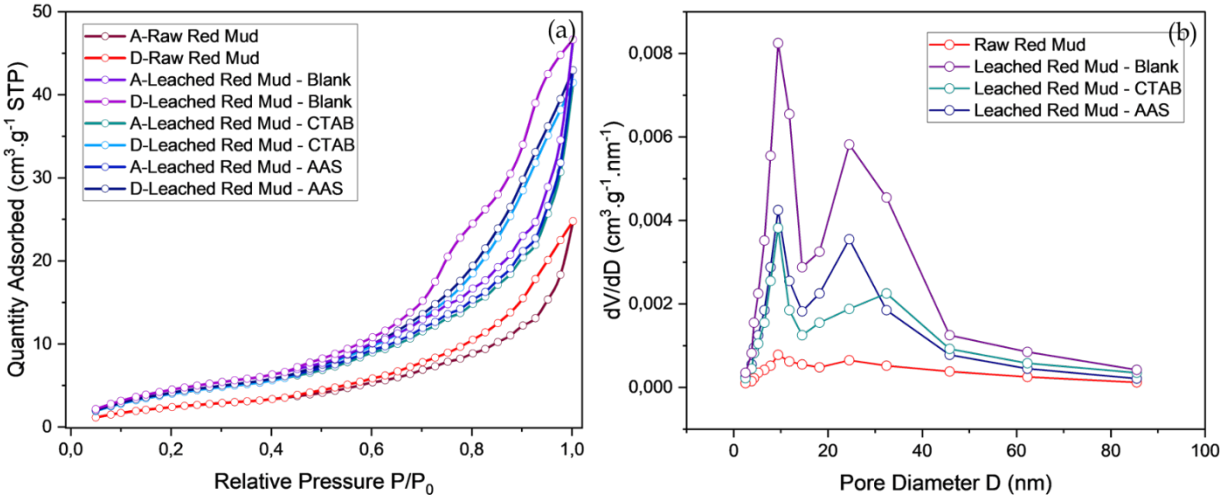

Fig. 10. BET-BJH analysis (a) Adsorption-desorption isotherms and (b) pore size distribution

Table 6. Textural properties of raw and leached red mud samples

Sample	S_{BET} (m^2 g^{-1})	V_P (cm^3 g^{-1})	D_{avg} (nm)
Raw Red Mud	11.41	0.038	13.4
Leached Blank	21.33	0.072	9.5
Leached CTAB Red Mud	19.01	0.064	11.2
Leached AAS Red Mud	19.68	0.066	10.8

Quantitatively, raw red mud exhibited a BET surface area (S_{BET}) of 11.41 m^2 g^{-1} and pore volume (V_P) of 0.038 cm^3 g^{-1}. Acid leaching without surfactant (blank) nearly doubled the S_{BET} (21.33 m^2 g^{-1}) and V_P (0.072 cm^3 g^{-1}), attributable to extensive dissolution of acid-soluble phases and formation of a porous framework. In contrast, surfactant-assisted system (CTAB–H_2SO_4 and AAS–H_2SO_4) showed slightly lower S_{BET} and V_P (19.01–19.68 m^2 g^{-1}; 0.064–0.066 cm^3 g^{-1}), likely due to partial pore blocking or surface coverage by adsorbed surfactant molecules, while still maintaining significantly higher porosity than the raw sample.

BJH pore size distribution (Fig. 10b) revealed the dominance of small mesopores in leached samples, consistent with the reduction in average pore diameter from 13.4 nm (raw) to 9.5–11.2 nm post-leaching. This shift reflects the generation of numerous new mesopores rather than pore shrinkage. The blank leached sample exhibited the highest pore population intensity, correlating with its maximum pore volume.

Confirmation of changes in mineralogical structure and their relationship to solubility selectivity was analyzed through the XRD pattern in Fig. 11. In the raw red mud sample, sharp and high-intensity diffraction peaks were observed at angles of approximately 24.2°, 33.2 °, 40.9 °, 49.5 °, and 54.1 °. The dominant peaks in the 33 °–36 ° area are generally associated with iron mineral phases such as hematite (Fe_2O_3), which are the main matrix components of red mud. In the blank leached sample, these peaks

were drastically attenuated or nearly vanished, representing severe destruction of the iron matrix due to aggressive acid attack. This extensive lattice breakdown explains the low selectivity of the blank system, as iron dissolution occurred concurrently with scandium extraction.

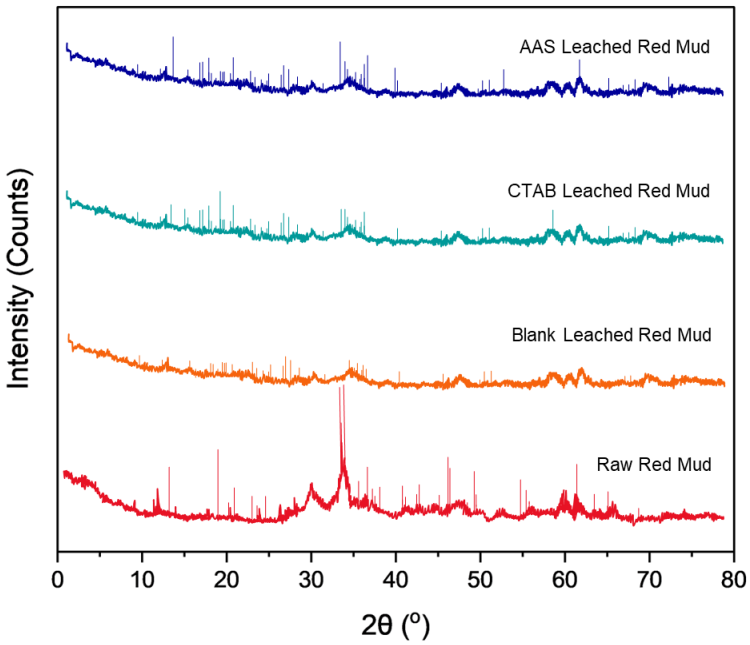

Fig. 11. Diffractogram of raw and leached red mud

Conversely, CTAB–H_2SO_4 and AAS–H_2SO_4 systems retained the main diffraction features, albeit with reduced intensity, demonstrating preservation of the iron matrix. Surfactants adsorb preferentially on Fe/Fe-oxide surfaces, forming a protective interfacial layer that suppresses acid-induced Fe dissolution through a corrosion-inhibition-like mechanism (Xiong et al., 2024; Lavanya et al., 2024). The surface passivation preserves the Fe mineral matrix while allowing selective leaching of more weakly bound metals, such as scandium, thereby enhancing Sc/Fe selectivity. Overall, surfactant-assisted leaching achieves an optimal balance between structural preservation and selective metal recovery, in contrast to the non-selective damage observed in the blank system.

3.7. Preliminary technoechonomic assessment: limitations and scope of scandium-only extraction

The preliminary technoeconomic assessment (TEA) presented in the flowchart in Fig. 12 is specifically designed to evaluate the extraction of scandium as the primary high-value target. Given the promising concentration of 119 ppm (as confirmed by ICP-MS analysis) and its premium market value exceeding USD 185,000/kg, this focused approach was intentionally selected to establish a conservative economic baseline. While realistic red mud processing inherently involves the recovery of major components such as iron (Fe), aluminum (Al), titanium (Ti), and silica (Si), their exclusion from the current incremental model (Fig. 12) ensures that the process's viability is tested under the most stringent conditions. Consequently, the profitability estimates provided are likely understated, as they do not yet account for the additional revenue streams from multi-metal recovery, which would further optimize the operational expenditures (OPEX) and the overall investment profile of the project.

The economic feasibility of the scandium recovery process was simulated using an incremental model, as conceptualized in Fig. 12. The simulation used a functional unit of 1,000 kg (1 metric ton) of bauxite residue (red mud) with a measured scandium concentration of 119 ppm. The performance metrics across three leaching scenarios are summarized in Table 7.

The results in Table 7 highlight the superior efficiency of the AAS-assisted system. By achieving a recovery of 73.93%, the AAS scenario yielded 103.29 g of scandium oxide (Sc_2O_3) as a final purified product per ton of red mud, significantly outperforming the Blank (74.76 g) and CTAB (94.67 g) systems. Despite the additional costs of synthesizing the AAS additive, the unit production cost for the AAS system is the lowest at 3.72 USD/g. This is a critical finding, as it proves that the chemical enhancement

not only improves technical recovery but also optimizes the overall economic burden. Furthermore, the highest Selectivity Ratio (1.33) achieved by AAS suggests a more refined pregnant leach solution (PLS), potentially reducing downstream purification expenses.

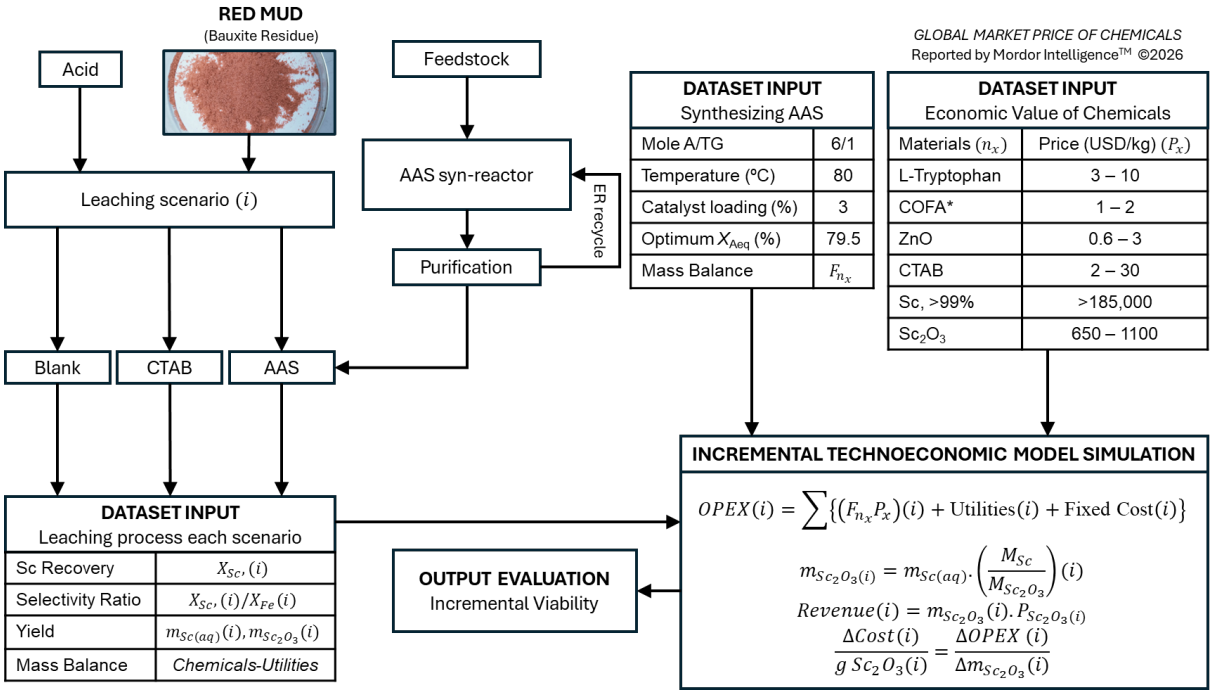

Fig. 12. Integrated framework for the preliminary technoeconomic assessment (TEA) and incremental viability simulation of scandium recovery

Table 7. Economic performance metrics (basis: 1,000 kg red mud, 119 ppm Sc)

Parameter	Unit	Blank	CTAB	AAS
Sc Recovery (X_{Sc})	%	53.51	67.76	73.93
Selectivity Ratio (X_{Sc}/X_{Fe})	-	0.62	0.94	1.33
Total Sc Recovered (m_{Sc}(aq))	g	63.68	80.63	87.95
Total Sc_2O_3 Yield	g	74.76	94.67	103.29
Total OPEX	USD	259.11	334.11	327.36
Unit Cost (Cost/g Sc_2O_3)	USD/g	4.07	4.14	**3.72**

To justify the strategic implementation of AAS, an incremental viability analysis was conducted to measure the cost-efficiency of adding the surfactant to the system (Table 8). As detailed in Table 8, transitioning from the Blank scenario to the AAS-assisted system requires an additional expenditure of USD 68.25 per ton of red mud. However, this investment yields an extra 28.53 grams of Sc_2O_3. The resulting incremental cost of 2.39 USD/g for this additional recovery is significantly lower than the unit cost of the blank process (3.77 USD/g), indicating high efficiency. Remarkably, compared to the commercial surfactant CTAB, the AAS system reduces OPEX by USD 6.75 while providing higher yield, resulting in a negative incremental cost (-0.78 USD/g).

This assessment confirms that the AAS-assisted leaching process is the most viable pathway for scandium recovery from red mud. By utilizing a waste-to-resource approach, the process reaches its viability, the lowest among all tested scenarios, reinforcing its potential for industrial-scale application.

Table 8. Incremental viability and efficiency analysis

Comparison	ΔOPEX (USD)	Δ$m$$Sc_2O_3$ Yield (g)	ΔCost/g (USD/g)
CTAB vs Blank	+75.00	19.88	3.77
AAS vs Blank	+68.25	28.53	2.39
AAS vs CTAB	-6.75	8.62	-0.78

3.8. Comparative environmental impact assessment (EIA) and integrated toxicity analysis

The environmental impact of processing 1 ton (1,000 kg) of red mud was assessed under three scenarios: Blank, CTAB, and AAS, focusing on inorganic acid waste, organic toxicity, and waste management. All scenarios used 1,500 kg of H_2SO_4 per ton of red mud, which can be neutralized with lime (CaO) to produce stable gypsum ($CaSO_4 \cdot 2H_2O$) (Eq. 18):

$$H_2SO_4 + CaO + H_2O \rightarrow CaSO_4 \cdot 2H_2O \quad (18)$$

Since no direct toxicity test was conducted on the synthesized AAS, the LC_{50} of the mixture was estimated using a component-based mass balance approach combined with instrumental characterization (^{1}H-NMR, GC–MS, FT-IR), as described in Eq. 19 to 21, using dataset (Table 9). The dose-response of each component was modeled using a Log-Logit function to predict the probability of effect (E_i) (substances i = 0–6), assuming additive or independent actions. The overall mixture effect (E_{mix}) was then calculated using the Independent Action (IA) model, where the survival probabilities of all components are multiplied (Wang et al., 2021).

$$E_i = \frac{1}{1+\left(\frac{LC_{50,i}}{C_i}\right)^{\beta}} \quad (19)$$

$$E_{mix} = 1 - \prod_{i=1}^{n}(1 - E_i) \quad (20)$$

$$0.5 = 1 - \prod_{i=1}^{n}\left(1 - \frac{1}{1+\left(\frac{LC_{50,i}}{LC_{50,AAS} \cdot y_i}\right)^{\beta}}\right) \quad (21)$$

where E_i = mortality for substance i (ranging from 0 to 1); $C_i = y_i(LC_{50,mix})$ = concentration of i within the mixture; $LC_{50,i}$ = the 50% lethal concentration for i; β = the slope of the dose-response curve = 2.0; y_i = mass fraction of i in the mixture; $LC_{50,mix}$ = target value LC_{50} of AAS.

Table 9. LC_{50} data for synthesized AAS toxicity calculation

Substances	i	y_i	Fish-Lethal concentration 50% (LC_{50})	
			Value (mg/L)	References for LC_{50}
COFA	0	0.368	1,000	(Das et al., 2022)
L-tryptophan	1	0.458	1,000–8,000	(Kalaiselvan et al., 2025)
Isopropanol *(trace)*	2	0.005	4,200–11,130	(ANZECC & ARMCANZ, 2020)
Acetone *(trace)*	3	0.001	2,100–16,700	(OECD, 1999)
Citric acid *(purified)*	4	0.001	440	(ESSECO S.r.l, 2020)
n-hexane *(trace)*	5	0.005	2.5	(Murugesu et al., 2019)
Zn *(residual)*	6	0.001	20	(Abdel-Khalek et al., 2015)

Volume affected water (VAT) was calculated assuming a surfactant dosage below the critical micelle concentration (CMC), corresponding to 5 kg (5,000,000 mg) per ton of red mud (Eq. 22). The VAT concept is consistent with risk-based approaches in life cycle impact assessment (LCIA), where environmental impact is expressed as the volume of water exposed to toxic concentrations affecting aquatic organisms. The results in Table 10 highlight the environmental impact of the three scenarios system.

$$\text{VAT (L)} = \frac{\text{Surfactant Load (mg)}}{LC_{50}(\text{mg/L})} \quad (22)$$

Even under conservative assumptions, AAS reduces ecological risk by more than >99% compared to CTAB in 1 ton of red mud leaching, while simultaneously improving metal recovery and process economics. Table 11 shows the integrated environmental profiles of the three scenarios.

Organic waste management differs significantly: CTAB (LC_{50}=0.3 mg/L) is highly stable and resistant to microbial degradation, requiring costly activated carbon filtration or advanced oxidation processes (AOPs) (Timer et al., 2019). Based on the calculation, 5 kg of CTAB per ton of red mud has the potential to contaminate up to 16.7 million liters of water to acute toxic levels (LC_{50}), equivalent to approximately 6–7 Olympic-sized swimming pools, assuming complete dispersion. In contrast, the same amount of AAS would only affect approximately 10,330 liters of water (10.33 m^3) based on calculated LC_{50} values, or up to 25,000 liters (25 m^3) under conservative assumptions. This corresponds to a volume comparable to a small household water tank. This stark difference demonstrates that AAS

reduces the potential aquatic impact by several orders of magnitude compared to CTAB, with affected water reduction (VAT_{red} > 99%), indicating a substantially lower environmental hazard.

Table 10. VAT and acute toxicity assessment

Scenario	LC_{50} (mg/L)	VAT (m^3)	Parameter	
Blank	N/A	N/A	Not applicable (no surfactant used in leaching)	
CTAB	0.3	16,667	VAT_{red} Equivalency Impact	: 0 (baseline) : 6–7 olympic pools : Severe (large scale water)
AAS (*calculated*)	483.9	10.33	VAT_{red} Equivalency $LC_{50\ AAS/CTAB}$ Impact	: 99.93% : 3–4 household water tanks : 1,613x (safer than CTAB) : Very low aquatic impact
AAS (*conservative*)	200	25	VAT_{red} Equivalency $LC_{50\ AAS/CTAB}$ Impact	: 99.85% : ±8 household water tanks : 666.67x : Low aquatic risk

Table 11. Integrated environmental profiles

Parameter	Blank	CTAB	AAS
Dominant waste type	Acid	Acid + toxic organics	Acid + biodegradable organics
Aquatic toxicity (LC_{50})	Not applicable	0.3 mg/L	200 – 484 mg/L
Volume affected water	Not applicable	16,667 m^3	10.33 – 25 m^3
Ease of handling	Very simple	Complex	Simple
Required treatment	Neutralization	Neutralization + AOPs	Neutralization + Bio-degradation

In conclusion, AAS is the optimal scenario, combining high Sc recovery (73.93%), strong economic performance (3.72 USD/g Sc_2O_3), and minimal toxic risk (extremely lower toxicity than CTAB). Its naturally biodegradable organic waste enables industrial application eco-friendly. The LC_{50} comparison (more than 99% reduction in volume affected water) strongly supports that AAS not only enhances Sc extraction but also substantially reduces ecological impact.

4. Conclusions

This study demonstrates that an amino acid-based surfactant (AAS) synthesized from L-tryptophan and COFA effectively enhances scandium (Sc) recovery from red mud by modifying solid-liquid interfacial properties. Kinetic analysis of AAS synthesis confirms that the reaction follows a pseudo-Langmuir model, with optimal performance achieved at 5 wt% ZnO catalyst loading. Interfacial thermodynamic evaluation reveals that AAS adsorption at the solid surface is thermodynamically more favorable than micellization ($\Delta G_{ads} < \Delta G_{mic}$), promoting strong interfacial activity under acidic leaching conditions. In hydrometallurgical application, the presence of AAS significantly improves Sc recovery and selectivity over Fe, while altering the leaching mechanism from surface reaction control to diffusion through the product layer, as validated by shrinking core modeling and activation energy analysis. Mineralogical and textural analyses further confirm that AAS mitigates excessive matrix dissolution, preserving the iron-rich structure while facilitating Sc extraction. Overall, AAS functions as an effective interfacial promoter rather than a simple wetting agent, offering a promising strategy for selective rare earth recovery from complex industrial residues such as red mud. AAS outperforms conventional surfactants in both environmental safety and economics. Its LC_{50} (200–484 mg/L) is over 667–1,613 times higher than CTAB (0.3 mg/L), promoting it far less toxic and naturally biodegradable, unlike conventional surfactants that persist and require costly treatments. Economically, AAS enables high scandium recovery (73.93%) with a production cost of 3.72 USD/g Sc_2O_3.

Acknowledgments

The authors gratefully acknowledge financial support from the Operational Assistance for State Universities program (BOPTN), Universitas Sumatera Utara (USU), Indonesia. The authors also thank all parties who provided technical assistance and facilities during the course of this research.

References

ABDEL-KHALEK, A.A., KADRY, M., HAMED, A., MARIE, M.-A., 2015. Ecotoxicological impacts of zinc metal in comparison to its nanoparticles in Nile tilapia (*Oreochromis niloticus*). *J. Basic Appl. Zool.* 72, 113–125.

AI, C.-M., SUN, P.-P., WU, A.-X., CHEN, X., LIU, C., 2019. *Accelerating leaching of copper ore with surfactant and the analysis of reaction kinetics.* Int. J. Miner. Metall. Mater. 26, 274–281.

ALAM, W.S., GITAMARA, S., WARTAKUSUMAH, R., NURDIN, M.I., MASYITHAH, Z., 2022. *Implementation of amino acid as a natural feedstock in production of N-acylamides as a biocompatible surfactants: A review on synthesis, behavioral, application and scale-up process.* J. Pure Appl. Chem. Res. 11(1).

ANZECC, ARMCANZ, 2000. *Australian and New Zealand Guidelines for Fresh and Marine Water Quality*. Canberra.

BORRA, C.R., BLANPAIN, B., PONTIKES, Y., BINNEMANS, K., VAN GERVEN, T., 2016a. *Smelting of bauxite residue (red mud) in view of iron and selective rare earths recovery.* Journal of Sustainable Metallurgy 2, 28–37.

BORRA, C.R., BLANPAIN, B., PONTIKES, Y., BINNEMANS, K., VAN GERVEN, T., 2016b. *Recovery of rare earths and other valuable metals from bauxite residue (red mud): A review.* Journal of Sustainable Metallurgy 2, 365–386.

DAS, A.K., SHILL, D.C., CHATTERJEE, S., 2022. Coconut oil for utility transformers – environmental safety and sustainability perspectives. *Renew. Sustain. Energy Rev.* 164, 112572.

ESSECO S.R.L., 2020. *Safety Data Sheet: Citric Acid*. Version 1, October 28, 2020.

HAFIDI, Z., GARCÍA, M.T., PONS, R., OLIVEIRA DE SOUSA, F.F., BAUTISTA, M.E., VÁZQUEZ, S., PÉREZ, L., 2025. *Green cationic phenylalanine and tryptophan-based surfactants: Influence of the polar head amino acids and hydrophobic character on the self-aggregation, antimicrobial activity, and environmental behavior.* J. Mol. Liq. 429, 127620.

HE, F., MA, B., QIU, Z., WANG, C., CHEN, Y., HU, X., 2023. *Enhanced extraction of nickel from limonitic laterite via improved nitric acid pressure leaching process.* Minerals Engineering 201, 108170.

HOLMBERG, K., BILÉN, F., BORDES, R., 2025. *Development of amino acid-based surfactants: From synthesis to applications.* Curr. Opin. Colloid Interface Sci. 75, 101884.

ISLAM, M.A., CHOWDHURY, M.A., MOZUMDER, M.S.I., UDDIN, M.T., 2021. *Langmuir adsorption kinetics in liquid media: Interface reaction model.* ACS Omega 6(22), 14481–14492.

JAVED, M., IQBAL, S., FATIMA, I., NADEEM, S., MOHYUDDIN, A., ARIF, M., AMJAD, A., SHAHID, S., ALSHAMMARI, F.H., ALAHMDI, M.I., ELKAEED, E.B., ALZHRANI, R.M., AWWAD, N.S., IBRAHIUM, H.A., QAYYUM, M.A., 2022. *Interactions between amino acids and a cationic surfactant in binary solvent system.* Colloid Interface Sci. Commun. 48, 100623.

JODŁOWSKI, P.J., JĘDRZEJCZYK, R.J., GANCARCZYK, A., ŁOJEWSKA, J., KOŁODZIEJ, A., 2017. *New method of determination of intrinsic kinetic and mass transport parameters from typical catalyst activity tests: Problem of mass transfer resistance and diffusional limitation of reaction rate.* Chem. Eng. Sci. 162, 322–331.

KALAISELVAN, P., RANJAN, A., THANGARANI, A.J., FELIX, N., AKAMAD, D.K., 2025. The fate of dietary tryptophan in fish: unveiling its sources, transport, metabolism, and multifaceted impacts. *J. Nutr.* 155(7), 2017–2042.

KALEBIC, D., BINNEMANS, K., DE WITTE, P.A.M., DEHAEN, W., 2023. *Synthesis, physicochemical characterization and aquatic toxicity studies of anionic surfactants derived from amino and a-hydroxy acids.* RSC Sustain. 1, 1995–2005.

KANEKAPUTRA, M.R., MUBAROK, M.Z., 2023. *Extraction of scandium from bauxite residue by high-pressure leaching in sulfuric acid solution.* Heliyon 9, e14652.

KAUR, R., KUMAR, H., KUMAR, B., SINGLA, M., KUMAR, V., GHFAR, A.A., PANDEY, S., 2022. *Effect of amino acid on the surface adsorption and micellar properties of surface active ILs varying in cationic head groups.* Heliyon 8(8), e10363.

KLAUBER, C., GRÄFE, M., POWER, G., 2011. *Bauxite residue issues: II. Options for residue utilization.* Hydrometallurgy 108, 11–32.

LAN, P., LUO, X., ZHANG, Y., LUO, P., TANG, X., 2025. *Enhanced leaching of ionic rare earth ore facilitated by sodium alcohol ether carboxylate surfactant.* J. Rare Earths 43, 2789–2798.

LAVANYA, M., MACHADO, A.A., 2024. *Surfactants as biodegradable sustainable inhibitors for corrosion control in diverse media and conditions: A comprehensive review.* Sci. Total Environ. 908, 168407.

LI, W., LI, Z., WANG, N., GU, H., 2022. *Selective extraction of rare earth elements from red mud using oxalic and sulfuric acids.* J. Environ. Chem. Eng. 10, 108650.

LIU, B., LUO, H., RONG, H., ZENG, X., WU, K., CHEN, Z., LU, H., XU, D., 2019. *Temperature-induced adsorption and desorption of phosphate on poly(acrylic acid-co-N-[3-(dimethylamino)propyl]acrylamide) hydrogels in aqueous solutions.* Desalin. Water Treat. 160, 260–267.

MURUGESU, S., KHATIB, A., AHMED, Q.U., IBRAHIM, Z., UZIR, B.F., BENCHOULA, K., YUSOFF, N.I.N., PERUMAL, V., ALAJMI, M.F., SALAMAH, S., EL-SEEDI, H.R., 2019. Toxicity study on *Clinacanthus nutans* leaf hexane fraction using *Danio rerio* embryos. *Toxicol. Rep.* 6, 1148–1154.

NIU, C., XIA, W., LI, Y., BU, X., WANG, Y., XIE, G., 2022. *Insight into the low-rank coal flotation using amino acid surfactant as a promoter.* Fuel 307, 121810.

OECD, 1999. *SIDS Initial Assessment Profile for Acetone (CAS No. 67-64-1).* SIAM 9, United States, 29 June–1 July 1999.

OKE, E.A., POTGIETER, H., MONDLANE, F., SKOSANA, N.P., TEIMOURI, S., NYEMBWE, J.K., 2024. *Concurrent leaching of copper and cobalt from a copper–cobalt ore using sulfuric and organic acids.* Minerals Engineering 216, 108853.

RAY, A.R., TRIPATHY, B.C., MISHRA, S., 2025. *Investigation on process optimization and kinetics for leaching of rare earth elements from red mud using citric acid.* Sci. Rep. 15, 36533.

RIVERA, R.M., OUNOUGHENE, G., BORRA, C.R., BINNEMANS, K., VAN GERVEN, T., 2017. *Neutralisation of bauxite residue by carbon dioxide prior to acidic leaching for metal recovery.* Miner. Eng. 112, 92–102.

SHOPPERT, A., LOGINOVA, I., NAPOL'SKIKH, J., KYRCHIKOV, A., CHAIKIN, L., ROGOZHNIKOV, D., VALEEV, D., 2022. *Selective scandium (Sc) extraction from bauxite residue (red mud) obtained by alkali fusion–leaching method.* Materials 15, 433.

TIMMER, N., GORE, D., SANDERS, D., GOUIN, T., DROGE, S.T.J., 2019. *Toxicity mitigation and bioaccessibility of the cationic surfactant cetyltrimethylammonium bromide in a sorbent-modified biodegradation study.* Chemosphere 222, 461–468.

WANG, Z. J., LIU, S. S., HUANG, P., XU, Y. Q., 2021. Mixture predicted no-effect concentrations derived by independent action model vs concentration addition model based on different species sensitivity distribution models. *Ecotoxicology and Environmental Safety* 227, 112898.

WELCH, J., WALLACE, J., LANSLEY, A.B., ROPER, C., 2021. *Evaluation of the toxicity of sodium dodecyl sulphate (SDS) in the MucilAir™ human airway model in vitro.* Regul. Toxicol. Pharmacol. 125, 105022.

WU, J., CHEN, A., PENG, S., WEI, Z., LIU, G., 2013. *Identification and application of amino acids as chelators in phytoremediation of rare earth elements lanthanum and yttrium.* Plant and Soil 373, 329–338.

XIONG, Y., CAO, M., 2024. *Application of surfactants in corrosion inhibition of metals.* Curr. Opin. Colloid Interface Sci. 73, 101830.

YAMAMOTO, T., KOBAYASHI, T., YOSHIKIYO, K., MATSUI, Y., TAKAHASHI, T., ASO, Y., 2009. *A ^{1}H NMR spectroscopic study on the tryptophan residues of lysozyme included by glucosyl-β-cyclodextrin.* J. Mol. Struct. 920(1–3), 264–269.

ZHANG, Y., ZHANG, B., YANG, S., ZHONG, Z., ZHOU, H., LUO, X., 2021. *Enhancing the leaching effect of an ion-absorbed rare earth ore by ameliorating the seepage effect with sodium dodecyl sulfate surfactant.* Int. J. Min. Sci. Technol. 31, 995–1002.

ZHOU, K., TENG, C., ZHANG, X., PENG, C., CHEN, W., 2018. *Enhanced selective leaching of scandium from red mud.* Hydrometallurgy 182, 57–63

ZHOU, F., ZHANG, L., WANG, Z., ZHANG, Y., CHI, R., WU, X., 2024. *Application of surfactant for improving leaching process of weathered crust elution-deposited rare earth ores.* Journal of Rare Earths 42, 181–190.

ZHOU, F., ZHANG, L., WANG, Z., ZHANG, Y., CHI, R., 2023. *Effect of surfactant addition on leaching process of weathered crust elution-deposited rare earth ores with magnesium sulfate.* Int. J. Min. Sci. Technol. 33, 1045–1053.